Hindawi
Mathematical Problems in Engineering
Volume 2021, Article ID 8837233, 12 pages
https://doi.org/10.1155/2021/8837233

Research Article

Incoherence Analysis of RD-AIC-Based Observation Matrix and Its Application in Power Quality Disturbance Signal

Yan Liu and Wei Tang

Department of Electrical and Control Engineering, Shaanxi University of Science and Technology, Xi'an 710021, China

Correspondence should be addressed to Yan Liu; liuyandq@sust.edu.cn

Received 6 September 2020; Revised 9 January 2021; Accepted 13 January 2021; Published 27 January 2021

Academic Editor: Jerzy Baranowski

In the theory of compressed sensing, restricted isometry property (RIP) decides the universality and reconstruction robustness of an observation matrix. At present, an observation matrix based on RD-AIC (RD-AIC-based observation matrix) can compress sparse continuous signals with a simple structure, but RIP analysis of this matrix is lack and challenging to prove. In this paper, this problem is relaxed. Instead, we demonstrate the incoherence analysis process, derive the orthogonality and nonsingularity of the matrix, propose the generalized relevance calculation steps of the matrix, and propose the hardware parameter design principles to improve the incoherence of the matrix. Moreover, compression and reconstruction experiments used in power quality disturbance signals are developed for testing the incoherence. The results show that the RD-AIC-based observation matrix has substantial incoherence under suitable hardware parameters, equivalent to the Gaussian random matrix and the Bernoulli random matrix.

1. Introduction

Compressed sensing (CS) is an efficient theory for signal compression [1], widely applied in medical imaging, radar imaging, and wireless sensors [2–4]. The classical CS theory is distributed CS, 1-bit CS, and blind CS [5–7], and the recent CS theory has developed with advanced control theory and deep learning technology. For example, Kyriadides [8] proposes an adaptive CS method to improve tracking performance, Palangi et al. [9] design a distributed CS with deep learning approach, and Wang et al. [10] introduce a method of combining convolutional neural network and CS. However, no matter what kind of CS theory, the observation matrix is an important part of obtaining sparse and compressible signal information. The restricted isometry property (RIP) is a standard tool for studying the universality and reconstruction robustness of an observation matrix [11]. Although Gaussian random matrix, Bernoulli random matrix, Toeplitz matrix, and Chaotic matrix [12–15] have been proved, which satisfied RIP, and are optimal for sparse recovery, they have limited use in practice because of complicated hardware structure, high complexity of calculation, and extensive expense on storage. Therefore, they are still stuck in theory and are only used to compress discrete signals:

$$y(m) = \Phi x(n), \tag{1}$$

where Φ is an observation matrix mentioned above, $x(n)$ is a discrete signal with sparsity, and $y(m)$ is a compressed sampling data.

An analog-to-information converter (AIC) is a vital under-sampling technique based on CS theory and samples the analog signals at the sub-Nyquist rate [16]. Recently, many AIC architectures have been designed in the literature, such as random demodulation AIC (RD-AIC) [17], modulated wideband converters (MWC) [18], and random modulation preintegrator (RMPI) [19]. Since RD-AIC has a broad application prospect with simple structure and low cost, it is usually used in practice to compress analog signals:

$$y(m) = \Phi_{\mathrm{RD-AIC}} x(t), \tag{2}$$

where Φ_{RD-AIC} is an observation matrix based on RD-AIC (RD-AIC-based observation matrix), $x(t)$ is an analog signal with sparsity, and $y(m)$ is a compressed sampling data.

Comparing equation (2) to equation (1), the RD-AIC-based observation matrix is significantly better than the traditional observation matrixes in engineering. Unfortunately, although many works discuss the structure and hardware implementation of an RD-AIC [20–22], few works discuss RIP of an RD-AIC-based observation matrix [23]. However, it is well known that RIP is an NP-hard problem to prove. Recently, some discriminating theorems instead of RIP property were proposed by some researchers [24, 25], which was to judge the incoherence of an observation.

This paper proposes to analyze the incoherence of RD-AIC-based observation matrix and apply it in power quality disturbance data. The main innovations and contributions of this work are as follows:

(1) A noncoherent analysis method based on the RD-AIC-based observation matrix is demonstrated to avoid an NP-hard problem for RIP proving

(2) An orthogonality and nonsingularity of RD-AIC-based observation matrix are deduced for the first time, solving the premise of applying discriminant theorems

(3) A design rule of hardware parameters is proposed, which can be used to enhance the incoherence of RD-AIC-based observation matrix

(4) Compression and reconstruction experiments used in power quality disturbance signals are developed for testing the incoherence

This paper is structured into five sections. The basic concepts and the mathematical model of the RD-AIC-based observation matrix are introduced in Section 2. In Section 3, we analyze the orthogonality and the nonsingularity of the RD-AIC-based observation matrix. We also propose the generalized relevance calculation step and the design principle to the RD-AIC-based observation matrix. The simulation experiment studies are exposed in Section 4. The conclusions are finally drawn in Section 5.

2. The Mathematical Model of RD-AIC-Based Observation Matrix

The structure of RD-AIC and RD-AIC-based observation matrix is shown in Figure 1. RD-AIC consists of signal modulation, low-pass filter (LPF), and uniform sampling at low speed, and the construction processing of Φ_{RD-AIC} is as follows.

It is assumed that an analog signal $x(t)$ is K sparse under the transform function $\varphi_n(t)$:

$$x(t) = \sum_{n=0}^{N-1} \alpha_n \varphi_n(t), \tag{3}$$

where α_n is the transforming factor, which has K nonzero values.

(1) $x(t)$ passes the signal modulation:

$$x_1(t) = x(t) p_c(t), \tag{4}$$

where $p_c(t)$ is a binary random sequence consisted of [-1, 1] and $x_1(t)$ is the output.

(2) $x_1(t)$ passes the LPF:

$$y_1(t) = \int_{-\infty}^{\infty} x(\tau) p_c(\tau) h(t-\tau) \mathrm{d}\tau, \tag{5}$$

where $h(t)$ is the unit impulse response of the LPF and $y_1(t)$ is the output. When equation (3) is substituted with (1), the following can be gained:

$$y_1(t) = \sum_{n=0}^{N-1} \alpha_n \int_{-\infty}^{\infty} \varphi_n(\tau) p_c(\tau) h(t-\tau) \mathrm{d}\tau. \tag{6}$$

(3) $y_1(t)$ passes the uniform sampling at low speed:

$$y(m) = \sum_{n=0}^{N-1} \alpha_n \int_{-\infty}^{\infty} \varphi_n(\tau) p_c(\tau) h(mT-\tau) \mathrm{d}\tau|_{t=mT}, \tag{7}$$

where T is a sampling interval, $0 \le m \le M-1$ and $M \ll N$, and $y(m) \in R^{M\times 1}$ is the output of RD-AIC.

Let

$$\theta_{m,n} = \int_{-\infty}^{\infty} \varphi_n(\tau) p_c(\tau) h(mT-\tau) \mathrm{d}\tau, \tag{8}$$

and there is

$$y(m) = \sum_{n=0}^{N-1} \theta_{m,n} \alpha_n = \Theta\alpha, \tag{9}$$

where $\alpha = [\alpha_1, \alpha_2, \ldots, \alpha_N]^T \in R^{N\times 1}$ and $\Theta \in R^{M\times N}$ is the integral result of the transformed function, the binary random sequence, and the unit impulse response. If the discretization is applied onto Θ, we obtain

$$\Theta = \mathrm{BHP}\Psi, \tag{10}$$

$$\Psi = \begin{bmatrix} \varphi_1(0) & \varphi_2(0) & \cdots & \varphi_{N-1}(0) \\ \varphi_1(1) & \varphi_2(1) & & \varphi_{N-1}(1) \\ \vdots & & \ddots & \vdots \\ \varphi_1(N-1) & \varphi_2(N-1) & \cdots & \varphi_{N-1}(N-1) \end{bmatrix}, \tag{11}$$

$$P = \begin{bmatrix} p_c(0) & 0 & \cdots & 0 \\ 0 & p_c(1) & & 0 \\ \vdots & & \ddots & \vdots \\ 0 & 0 & \cdots & p_c(N-1) \end{bmatrix}, \tag{12}$$

$$H = \begin{bmatrix} h(0) & 0 & 0 & \ldots & \ldots & 0 \\ h(1) & h(0) & 0 & \ldots & \ldots & 0 \\ h(2) & h(1) & h(0) & \ldots & \ldots & 0 \\ \vdots & \ddots & \ddots & \ddots & 0 & 0 \\ \vdots & \ldots & \ldots & h(1) & h(0) & 0 \\ h(N-1) & \ldots & \ldots & h(2) & h(1) & h(0) \end{bmatrix}, \tag{13}$$

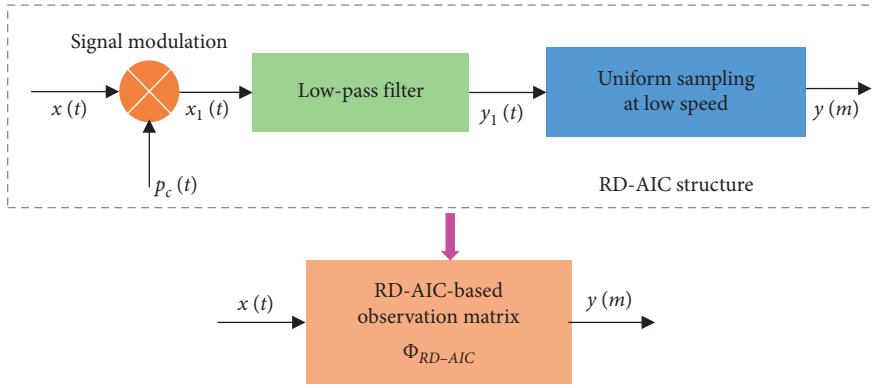

Figure 1: The structure of RD-AIC and the RD-AIC-based observation matrix.

$$B = \oplus_{m=0}^{M-1}\kappa \in \{0,1\},$$
$$\kappa = \begin{cases} 1, & n = C, \\ 0, & n \neq C, \end{cases} \tag{14}$$

where $\Psi \in R^{N\times N}$ is the transform function matrix that is consisted of the discretized $\varphi_n(n)$, $P \in\in R^{N\times N}$ is the binary random sequence matrix that is consisted of the discretized $p_c(n)$, $H \in R^{N\times N}$ is the unit impulse response matrix that is consisted of the circular movement of the discretized $h(n)$, and $B \in\in R^{M\times N}$ is the uniform sampling matrix consisted of the direct sum of M same κ vectors.

According to equation (10) and CS principle [1], $\Phi_{\text{RD–AIC}}$ is

$$\Phi_{\text{RD–AIC}} = \text{BHP}, \tag{15}$$

where $\Phi_{\text{RD–AIC}} \in R^{M\times N}$ and $c = (M/N) \times 100\%$ is the compression ratio. The smaller the value of c, the less the number of samples.

3. Analysis Method of Incoherence

3.1. Relevance Discriminating Theorem

Theorem 1. *If an observation matrix Φ is constructed byM rows of vectors which are randomly drawn from an orthogonal matrix $\Phi_Z = [\phi_{Z1}, \phi_{Z2}, \ldots, \phi_{ZN}] \in R^{N\times N}$, the sufficient condition which allows solving reconstruction by a norm optimization method is*

$$M \geq lu^2(\Phi_Z, \Psi)\frac{K}{\log(N)}, \tag{16}$$

where l is the constant, $u \in [1, \sqrt{N}]$ is the relevance between the orthogonal matrix Φ_Z, and the transform function matrix Ψ:

$$u(\Phi_Z, \Psi) = \sqrt{N}\max_{i,j}\left|\langle\phi_{Zi}, \varphi_j\rangle\right|. \tag{17}$$

Theorem 2. *If an observation matrix $\widehat{\Phi}$ is constructed by M rows which are drawn randomly from a nonsingular matrix $\widehat{\Phi}_Z = [\widehat{\phi}_{Z1}, \widehat{\phi}_{Z2}, \ldots, \widehat{\phi}_{ZN}] \in R^{N\times N}$, then the sufficient condition which allows solving reconstruction by a norm optimization method is*

$$M \geq l\widehat{u}^2\left(\widehat{\Phi}_Z, \Psi\right)\frac{K}{\log(N)}, \tag{18}$$

where $\widehat{u} \in [1, \sqrt{N}]$ is the generalized relevance between the nonsingular matrix $\widehat{\Phi}_Z$ and the transform function matrix Ψ:

$$\widehat{u}\left(\widehat{\Phi}_Z, \Psi\right) = \sqrt{N}\max_{i,j}\left|\langle\widehat{\phi}'_{Zi}, \varphi_j\rangle\right|, \tag{19}$$

where $\widehat{\phi}'_{Z1}, \widehat{\phi}'_{Z2}, \ldots, \widehat{\phi}'_{ZN}$ is the group of the orthogonal base function corresponded by Schimidt orthogonal unitized $\widehat{\phi}_{Z1}, \widehat{\phi}_{Z2}, \ldots \widehat{\phi}_{ZN}$.

Theorems 1 and 2 show that an observation matrix with a great incoherence can gain less compressed observation values and strong reconstruction robustness and vice versa. The difference between the two theorems is that an orthogonal matrix constructs the observation matrix in Theorem 1, while a nonsingular matrix builds the observation matrix in Theorem 2.

3.2. Analysis of the Orthogonality and Nonsingularity.

Let

$$\Phi_{\text{HP}} = \text{HP}, \tag{20}$$

where $\Phi_{\text{HP}} \in R^{N\times N}$ is the part of the RD-AIC-based observation matrix $\Phi_{\text{RD–AIC}}$.

According to equation (15), $\Phi_{\text{RD–AIC}}$ is constructed by M rows which are drawn randomly from the square matrix Φ_{HP}. Therefore, to use the above theorems, the orthogonality and nonsingularity of Φ_{HP} need to be analyzed.

According to equations (12) and (13),Φ_{HP} can be drawn:

$$\Phi_{\mathrm{HP}} = \begin{bmatrix} p_c(0)h(0) & 0 & 0 & \cdots & \cdots & 0 \\ p_c(0)h(1) & p_c(1)h(0) & 0 & \cdots & \cdots & 0 \\ p_c(0)h(2) & p_c(1)h(1) & p_c(2)h(0) & \cdots & \cdots & 0 \\ \vdots & \ddots & \ddots & \ddots & 0 & 0 \\ \vdots & \ddots & \ddots & \ddots & p_c(N-2)h(0) & 0 \\ p_c(0)h(N-1) & \cdots & \cdots & \cdots & p_c(N-2)h(1) & p_c(N-1)h(0) \end{bmatrix}, \tag{21}$$

where Φ_{HP} is the triangular matrix without the orthogonality.

The nonsingularity of Φ_{HP} depending on the diagonal element is zero. Because $p_c(m)$ is not equal to zero, the nonsingularity of Φ_{HP} relies on the first value of $h(n)$.

According to the LPF design theory, many prototype filters have different structures, for example, Butterworth, Chebyshev, and ellipse. Recently, the fractional-order idea is used in the LPF design [26–28]. The order and the parameter number of the filters mentioned above are not the same, which undoubtedly increases the difficulty of deriving the first value of $h(n)$.

As it is well known, the ideal LPF is nonrealizable. However, the results of its research can be used to guide the design of actual filters. Therefore, in order to facilitate the analysis, we replaced the actual filter with the ideal filter and assumed that Φ_{HP} is consisted of a binary random sequence matrix and an ideal unit impulse response matrix.

Then, let

$$\Phi'_{\mathrm{HP}} = \begin{bmatrix} p_c(0)h'(0) & 0 & 0 & \cdots & \cdots & 0 \\ p_c(0)h'(1) & p_c(1)h'(0) & 0 & \cdots & \cdots & 0 \\ p_c(0)h'(2) & p_c(1)h'(1) & p_c(2)h'(0) & \cdots & \cdots & 0 \\ \vdots & \ddots & \ddots & \ddots & 0 & 0 \\ \vdots & \ddots & \ddots & \ddots & p_c(N-2)h'(0) & 0 \\ p_c(0)h'(N-1) & \cdots & \cdots & \cdots & p_c(N-2)h'(1) & p_c(N-1)h'(0) \end{bmatrix}, \tag{22}$$

where $\Phi'_{\mathrm{HP}} \in R^{N\times N}$ is also the triangular matrix without orthogonality, $h'(n)$ is the ideal unit impulse response of the LPF, and its mathematical model is

$$h'(n) = \frac{\sin(\pi n/T)}{\pi n/T}, \tag{23}$$

where $h'(n)$ is the *sinc* function and $h'(0)$ is not equal to zero, as shown in Figure 2.

Hence, Φ'_{HP} is the nonsingular matrix and available to implement generalized irrelevance analysis with Theorem 2.

3.3. Generalized Relevance Calculation and Design Principle. Based on Theorem 2, the generalized relevance calculation step of Φ'_{HP} is shown in Table 1, and the calculation results under the different parameters have been provided in Figure 3.

Besides, to comprehensively study the incoherence of Φ'_{HP}, the statistics mean $\widehat{u}_{\mathrm{mean}}$ and the statistics fluctuation value β are defined as

$$\widehat{u}_{\mathrm{mean}} = \frac{1}{L}\sum_{i}^{L}\widehat{u}_i, \qquad \beta = \max\left(\left|\frac{(\widehat{u}_i - \widehat{u}_{\mathrm{mean}})}{\widehat{u}_{\mathrm{mean}}}\right|\right), \tag{24}$$

where $\widehat{u}_i$ is the ith generalized relevance and L is the statistic times. If $\widehat{u}_{\mathrm{mean}} \ll \sqrt{N}$, it indicates a stronger incoherence of Φ'_{HP}. If β is small, it shows less fluctuation and better stability. Calculation of the statistical results under different parameters is shown in Table 2.

Above the calculation and statistical results imply the trend of how to increase the incoherence of Φ'_{HP}. It also shows how to enhance reconstruction robustness and compression ratio to the RD-AIC-based observation matrix. The details and parameter design principles are as follows:

(1) There is a relationship that exists between $\widehat{u}$ and T_p. Both $\widehat{u}_{\mathrm{mean}}$ and β will increase along with the dropping of T_p at the same f_p. Therefore, T_p should be extended as long as possible at the prerequisite of the hardware cost of the guaranteed RD-AIC-based observation matrix.

(2) There is a relationship that exists between $\widehat{u}$ and f_p. Both $\widehat{u}_{\mathrm{mean}}$ and β will augment along with the dropping of f_p at the same T_p. Therefore, f_p increase appropriately can enhance the performance of the RD-AIC-based observation matrix. However, f_p can be constricted without demolishing the stronger incoherence when T_p is bigger.

(3) There is no relation existed between $\widehat{u}$ and T. T is only relative to the compression rate c. Therefore, the

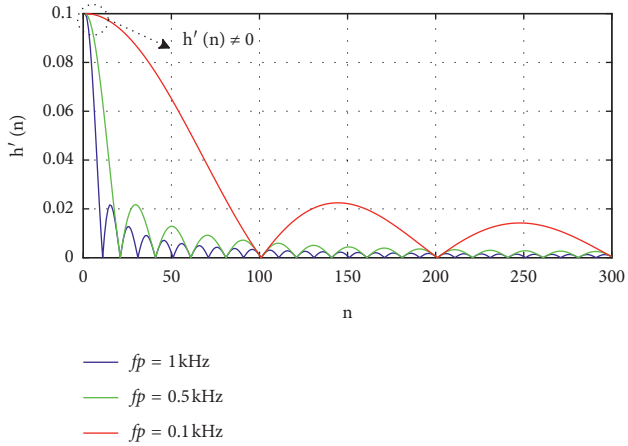

Figure 2: Unit impulse response of the ideal LPF under different passband cut-off frequencies f_p.

Table 1: The generalized relevance calculation step based on Theorem 2.

The calculation step
Step 1: set period of the binary random sequence T_p and the passband cut-off frequency f_p
Step 2: construct the binary random sequence $p_c(n)$ and the ideal unit impulse response $h'(n)$
Step 3: construct Φ_{HP}' based on equation (20)
Step 4: conduct Schimidt orthogonalization on column vectors in Φ_{HP}' to get standard orthogonal bases $\widehat{\phi}_{HP1}', \widehat{\phi}_{HP2}', \ldots, \widehat{\phi}_{HPN}'$
Step 5: calculate the generalized relevance $\widehat{u}$ based on equation (17)

augmentation of c is required, and f_p can be restricted appropriately with the prerequisites of (a) and (b) which are satisfied.

4. Experiment

In this section, to verify the compression and reconstruction performance, the RD-AIC-based observation matrix with the design principle mentioned above is applied to the power quality disturbance signal. Meanwhile, the mean absolute error (*MAE*), the mean squared error (*MSE*), and the compression rate c have been adopted.

4.1. Voltage Sag Experiment. The voltage sag refers to a sudden dropping of mean squared values of power frequency voltage at a certain point in the power grid and returning to normal after a short duration [29]. According to IEEE Electromagnetic Compatibility Standard, the normalized mathematical expression of the voltage sag is

$$x(t) = \cos(2\pi f t)\left(1 - a_1 u(t - t_1) - u(t - t_2)\right), \quad (25)$$

where f is the frequency of the base wave in the power grid, $a_1 \in [0.1, 0.9]$ is the depth of the voltage sag, t_1 is the initiation time, and t_2 is the ending time.

Let $a_1 = 0.3$, $t_1 = 41.2$ ms, $t_2 = 123$ ms, $T = 0.5$ ms, $N = 2000$, $T_p = 1000$, $f_p = 1$ KHz, and $M = 400$. The compression sampling processing that the voltage sag signal passes through each part of RD-AIC-based observation matrix is shown in Figure 4.

The time-frequency comparison between the reconstructed signal and the original signal is shown in Figure 5. It can be spotted a good reconstruction performance. Also, the experiment is implemented under different T_p, f_p, and white Gaussian noise. Furthermore, the results are shown in Table 3, where each index statistic is the mean of 100 parallel experiments.

4.2. Harmonic Experiment. The harmonic is commonly generated by the nonlinear loadings in the power users [30]. According to IEEE Electromagnetic Compatibility Standard, the mathematical expression of the normalized amplitudes of harmonic is

$$x(t) = \cos(2\pi f t) + \sum a_2 \cos(2\pi f_i t), \quad (26)$$

where a_2 is the amplitude of harmonic and f_i is the frequency of harmonic.

Let $f_i = 85$ Hz, 150 Hz, 350 Hz and the other parameter setting of T_p, f_p, f_s, M, and c be the same as the voltage sag experiment. The harmonic signal passing through each part of the RD-AIC-based observation matrix is shown in Figure 6.

The time-frequency comparison between the reconstructed signal and the original signal is shown in Figure 7. It also can be spotted as a good reconstruction performance. The results of the comparison experiment under different parameters are shown in Table 4.

4.3. Data Analysis. According to Tables 3 and 4, the decreasing tendency of *MAE* and *MSE* is denoted along with the increase of *SNR*, yet the reconstruction performance is different evidently under different T_p and f_p. To simplify, in this section, only *MSE* is compared and analyzed, and the different *MSE* curves are shown in Figures 8 and 9.

The analysis results of Figures 8 and 9 are as follows:

(1) When $T_p = 1000$, *MSE* is all little under different f_p and *SNR* and the maximum *MSE* is not more than $1e-02$. It indicates that even if f_p is significantly reduced, the RD-AIC-based observation matrix still has outstanding reconstruction performance and robustness against noise with a bigger T_p.

(2) When $T_p = 31$, *MSE* drops along with the ascending f_p and the minimum *MSE* is $4.35e-0.4$. It indicates that there is still excellent reconstruction performance and robustness against noise with a smaller T_p and a bigger f_p.

(3) When $T_p = 7$, MSE is all big under any f_p and SNR and the minimum MSE is 0.1977. It indicates that even if f_p is significantly increased, the RD-AIC-based observation matrix still has worse reconstruction performance and robustness against noise with a very small T_p.

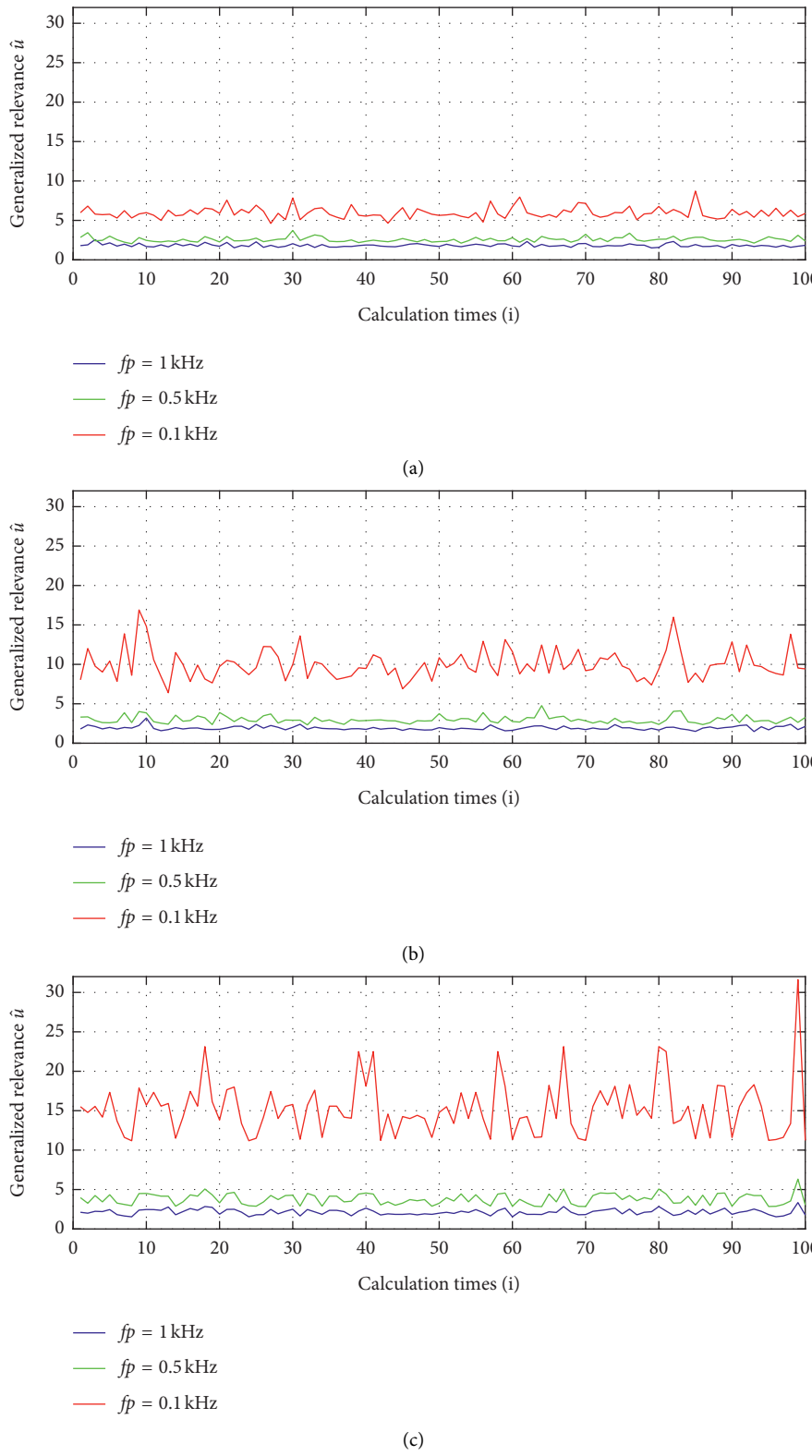

FIGURE 3: The generalized relevance calculation results of Φ_{HP}' under the different parameters. (a) The results under $T_p = 1000$, (b) the results under $T_p = 31$, and (c) the results under $T_p = 7$.

The above analysis results are consistent with the statistics results on incoherence in Section 3.3, verifying this paper's content.

4.4. Comparison with the Random Observation Matrix. The RD-AIC-based observation matrix has been compared with Gaussian random matrixes and Bernoulli random

Table 2: The generalized relevance statistical results of Φ_{HP}' under the different parameters.

Statistical results	$T_p = 1000$			$T_p = 31$			$T_p = 7$		
	1 *kHz*	0.5 *kHz*	0.1 *kHz*	1 *kHz*	0.5 *kHz*	0.1 *kHz*	1 *kHz*	0.5 *kHz*	0.1 *kHz*
$\widehat{u}_{\text{mean}}$	1.845	2.592	6.028	1.992	2.943	9.785	2.147	3.796	15.288
β	0.280	0.286	0.329	0.501	0.575	0.568	0.562	0.666	1.068

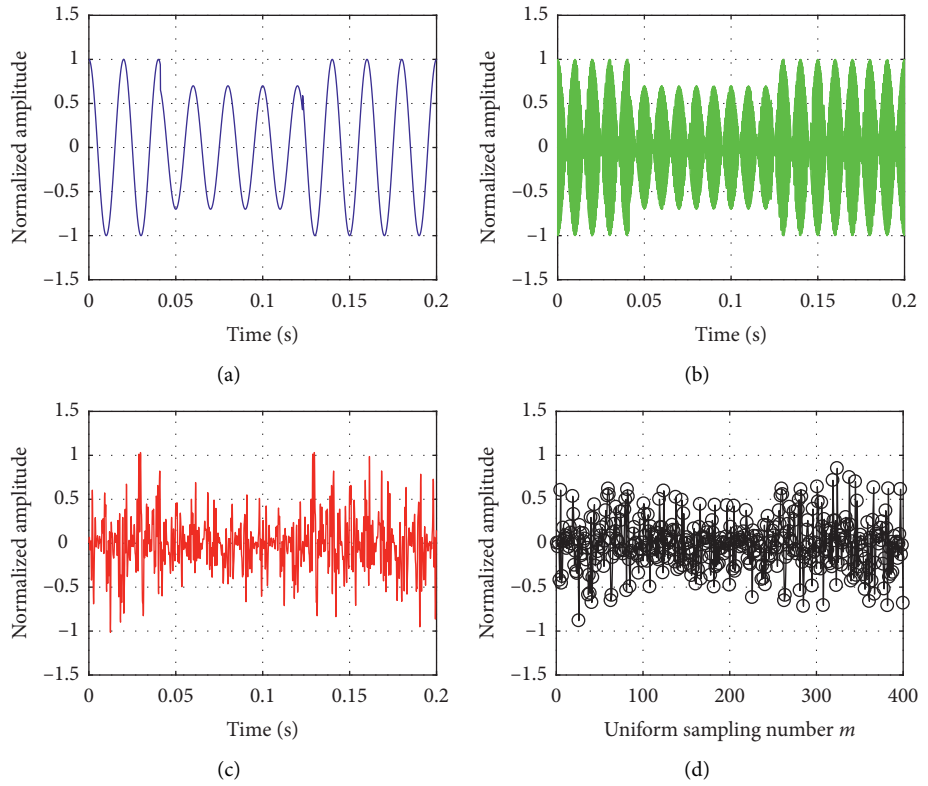

Figure 4: The compression sampling process of the voltage sag signal passing through the RD-AIC-based observation matrix. (a) The original signal, (b) the modulated signal, (c) the filtered signal, and (d) the compressed sampling signal.

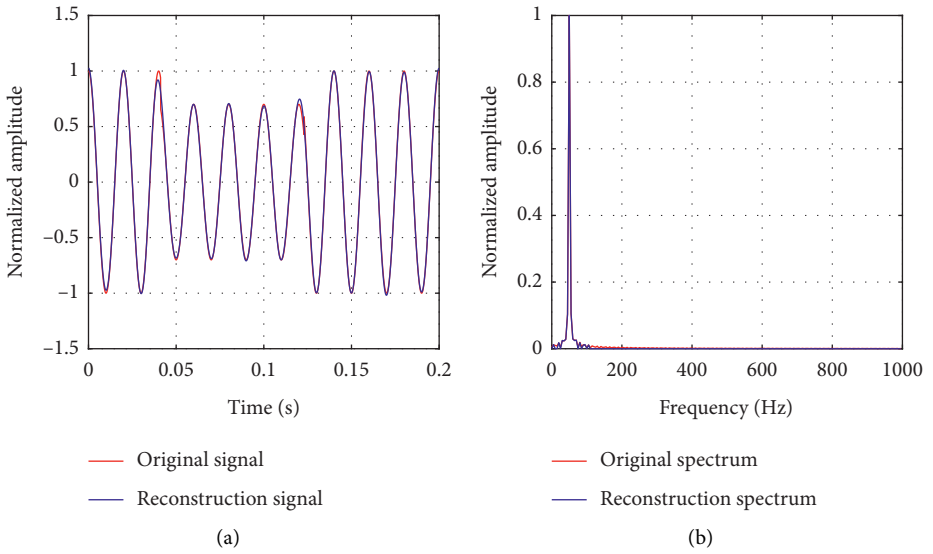

Figure 5: The time-frequency comparison between the reconstruction voltage sag signal and the original voltage sag signals. (a) The time domain. (b) The frequency domain.

Table 3: The reconstruction performance comparison under different parameters.

$f_p(kHz)$	SNR (dB)	$T_p = 1000$		$T_p = 31$		$T_p = 7$	
		MAE	MSE	MAE	MSE	MAE	MSE
1	20	0.059	0.0055	0.051	0.050	0.463	0.3126
	25	0.028	0.0014	0.027	$4.2e-03$	0.360	0.3756
	30	0.018	$5.94e-04$	0.080	$2.4ee-03$	0.362	0.2956
	35	0.012	$5.10e-04$	0.038	$1.3e-03$	0.363	0.2925
	40	0.013	$4.89e-04$	0.013	$4.35e-04$	0.267	0.1977
0.5	20	0.053	$4.6e-03$	0.266	0.2046	0.575	0.4478
	25	0.039	$2.8e-03$	0.167	0.1165	0.465	0.3885
	30	0.022	$1.0e-03$	0.148	0.1082	0.441	0.3804
	35	0.017	$6.47e-04$	0.133	0.0981	0.483	0.3686
	40	0.015	$5.95e-04$	0.131	0.0992	0.428	0.3536
0.1	20	0.081	0.0106	0.388	0.3325	0.504	0.4294
	25	0.057	$5.3e-03$	0.385	0.3046	0.472	0.3781
	30	0.042	$3.1e-03$	0.378	0.2952	0.438	0.3517
	35	0.039	$2.8ee-03$	0.347	0.2828	0.414	0.3420
	40	0.033	$2.3e-03$	0.266	0.2075	0.407	0.3291

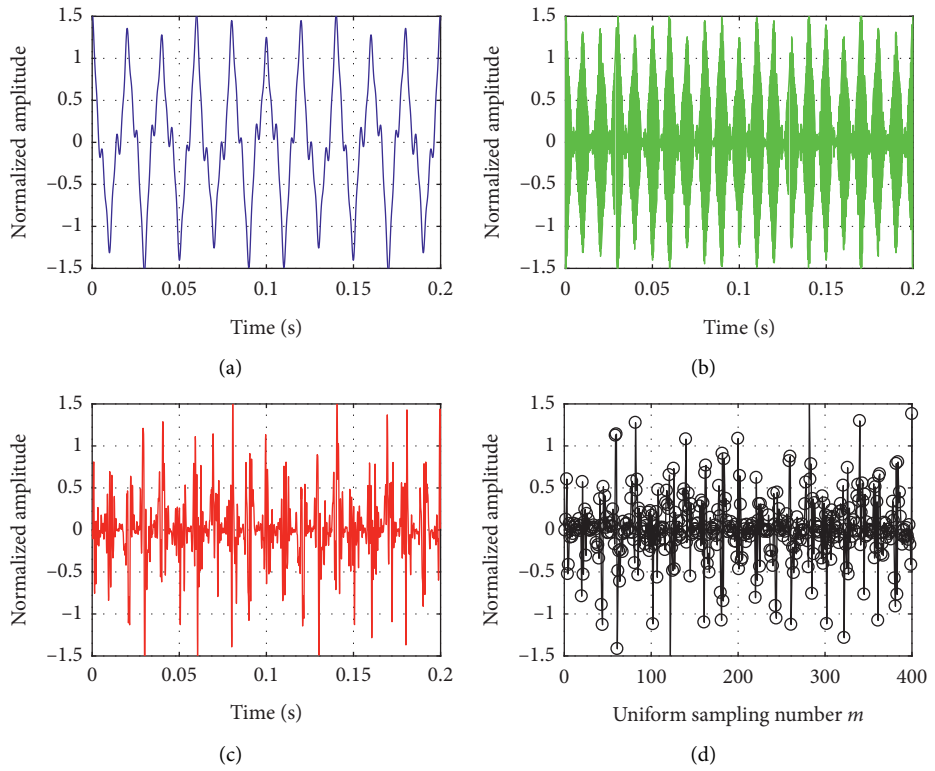

Figure 6: The compression sampling process of the harmonic passing through the RD-AIC-based observation matrix. (a) The original signal, (b) the modulated signal, (c) the filtered signal, and (d) the compressed sampling signal.

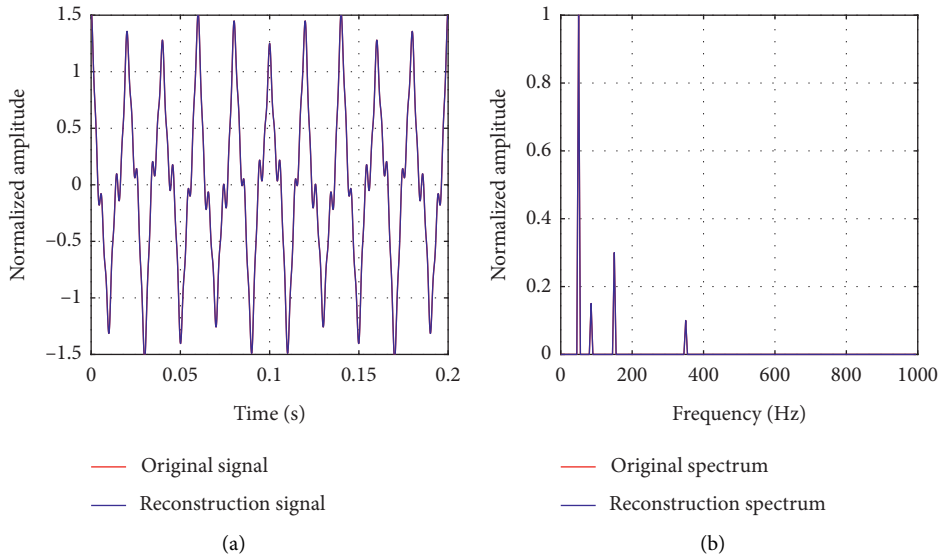

Figure 7: The time-frequency comparison between the reconstruction harmonic signal and the original harmonic signals. (a) The time domain. (b) The frequency domain.

Table 4: The reconstruction performance comparison under different parameters.

$f_p(kHz)$	$SNR\ (dB)$	$T_p = 1000$		$T_p = 31$		$T_p = 7$	
		MAE	MSE	MAE	MSE	MAE	MSE
1	20	0.061	$7.8e-03$	0.084	0.0159	0.520	0.5228
	25	0.044	$5.2e-03$	0.064	$9.9e-03$	0.517	0.4809
	30	0.042	$4.9e-03$	0.061	$9.2e-03$	0.486	0.4956
	35	0.040	$4.8e-03$	0.047	$5.6e-03$	0.458	0.4369
	40	0.040	$4.8e-03$	0.045	$5.2e-03$	0.385	0.3049
0.5	20	0.071	0.0101	0.369	0.3861	0.6317	0.6902
	25	0.051	$6.1e-03$	0.358	0.3260	0.589	0.6657
	30	0.044	$5.4e-03$	0.233	0.1884	0.580	0.6863
	35	0.043	$5.1e-03$	0.192	0.1153	0.557	0.5906
	40	0.040	$5.1e-03$	0.140	0.0841	0.405	0.4734
0.1	20	0.126	0.0274	0.5483	0.5785	0.660	0.7752
	25	0.118	0.0256	0.557	0.5763	0.644	0.7259
	30	0.105	0.0222	0.543	0.5722	0.644	0.7217
	35	0.082	0.0149	0.498	0.5075	0.617	0.6503
	40	0.079	0.0153	0.479	0.4229	0.510	0.5052

matrixes at different c (2%, 4%, 5%, 10%, 20%, 25%, 30%, 35%, 40%, and 50%). The comparison results are shown in Figure 10. An obvious reconstruction error only occurs under c at 2%. However, under other c, the reconstruction performance is similar to the Gaussian random matrix and Bernoulli random matrix. In summary, an RD-AIC-based observation matrix following the design principle is sufficient to realize the highly precious reconstruction at high compression ratios. It is equivalent to that of the classical Gaussian random matrix and Bernoulli random matrixes.

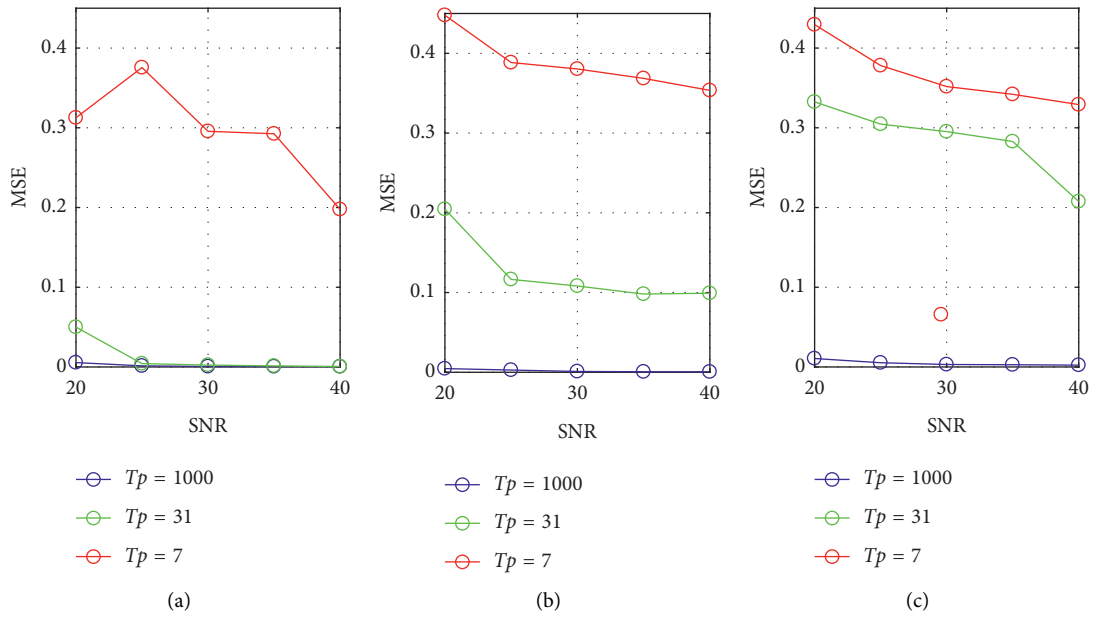

FIGURE 8: The reconstruction performance comparison of the voltage sag experiment at the parameters f_p, T_p, and SNR. (a) Different MSE curve under $f_p = 1$ KHz. (b) Different MSE curve under $f_p = 0.5$ KHz. (c) Different MSE curve under $f_p = 0.1$ KHz.

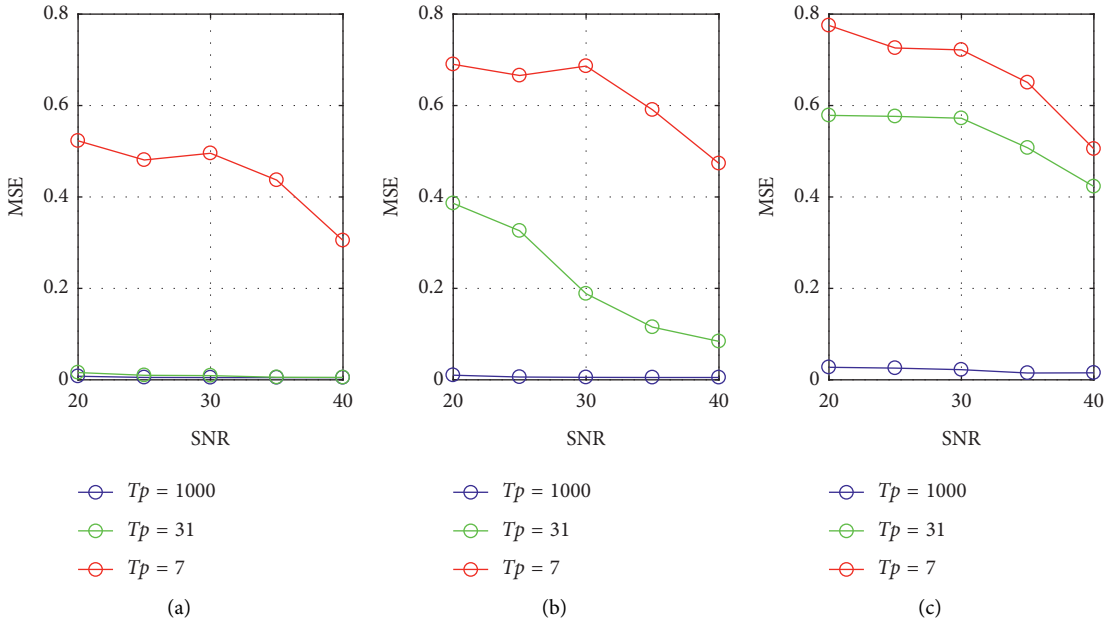

FIGURE 9: The reconstruction performance comparison of the harmonic experiment at the parameters f_p, T_p, and SNR. (a) The different MSE curve under $f_p = 1$ KHz. (b) The different MSE curve under $f_p = 0.5$ KHz. (c) The different MSE curve under $f_p = 0.1$ KHz.

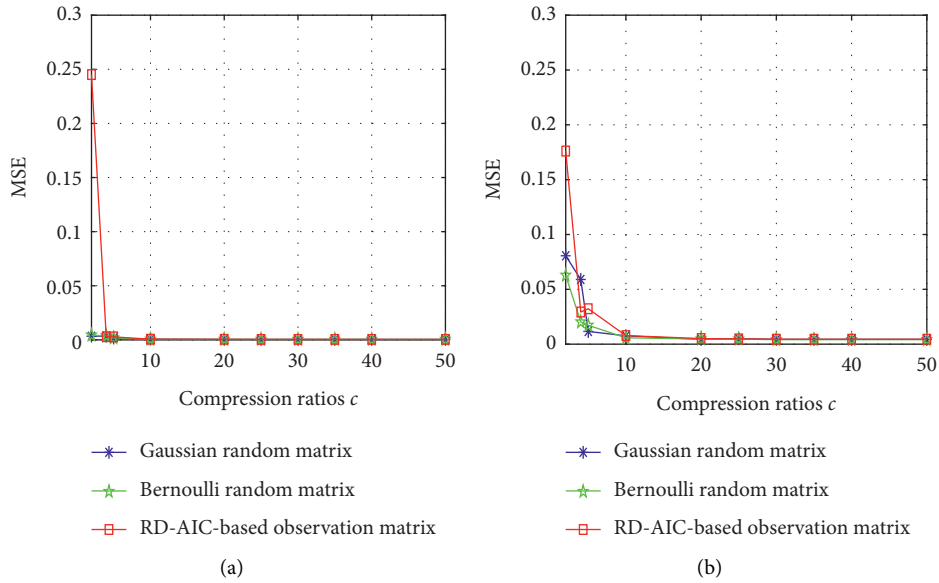

Figure 10: The reconstruction performance comparison of using the different observation matrices. (a) The reconstruction comparison of the voltage sag. (b) The reconstruction comparison of the harmonic.

5. Conclusions

The work in this paper provides a theoretical and technical reference for incoherence analysis of the RD-AIC-based observation matrix. Some conclusions are shown as follows:

(1) The square matrix of the RD-AIC-based observation matrix based on the binary random sequence and the ideal low-pass filter unit impulse response is not orthogonal but nonsingular

(2) The incoherence of the RD-AIC-based observation matrix is related to the binary random sequence period and the passband cut-off frequency of LPF

(3) The RD-AIC-based observation matrix with substantial incoherence is suitable for power quality disturbance data and is great as the Gaussian random matrix and Bernoulli random matrix on reconstruction performance

Data Availability

The data used to support the findings of this study are available from the corresponding author upon request.

Conflicts of Interest

The authors declare that they have no conflicts of interest.

Acknowledgments

This study was supported by the Natural Science Basic Research Plan in Shaanxi Province of China (Program no. S2019-JC-QN-0711) and Light Industry Intelligent Detection and Control Innovation Team (Program no. AI2019005).

References

[1] D. Donoho, "Compressed sensing," *IEEE Transactions on Information Theory*, vol. 52, no. 4, pp. 1280–1306, 2006.

[2] T. M. Quan, T. Nguyen-Duc, and W.-K. Jeong, "Compressed sensing MRI reconstruction using a generative adversarial network with a cyclic loss," *IEEE Transactions on Medical Imaging*, vol. 37, no. 6, pp. 1488–1497, 2018.

[3] M. Becquaert, E. Cristofani, B. Lauwens, M. Vandewal, J. H. Stiens, and N. Deligiannis, "Online sequential compressed sensing with multiple information for through-the-wall radar imaging," *IEEE Sensors Journal*, vol. 19, no. 11, pp. 4138–4148, 2019.

[4] M. Leinonen, M. Codreanu, and M. Juntti, "Distributed distortion-rate optimized compressed sensing in wireless sensor networks," *IEEE Transactions on Communications*, vol. 66, no. 4, pp. 1609–1623, 2018.

[5] S. Patterson, Y. C. Eldar, I. Keidar, and I. Keidar, "Distributed compressed sensing for static and time-varying networks," *IEEE Transactions on Signal Processing*, vol. 62, no. 19, pp. 4931–4946, 2014.

[6] L. Jacques, J. N. Laska, P. T. Boufounos, and R. G. Baraniuk, "Robust 1-bit compressive sensing via binary stable embeddings of sparse vectors," *IEEE Transactions on Information Theory*, vol. 59, no. 4, pp. 2082–2102, 2013.

[7] S. Gleichman and Y. C. Eldar, "Blind compressed sensing," *IEEE Transactions on Information Theory*, vol. 57, no. 10, pp. 6958–6975, 2011.

[8] L. Kyriadides, "Target tracking using adaptive compressive sensing and processing," *Signal Processing*, vol. 127, pp. 44–55, 2016.

[9] H. Palangi, R. Ward, and L. Deng, "Distributed compressive sensing: a deep learning approach," *IEEE Transactions on Signal Processing*, vol. 64, no. 17, pp. 4504–4518, 2016.

[10] Y. Wang, J. Yang, M. Liu, and G. Gui, "LightAMC: lightweight automatic modulation classification via deep learning and compressive sensing," *IEEE Transactions on Vehicular Technology*, vol. 69, no. 3, pp. 3491–3495, 2020.

[11] H. Zhao, L. Zhang, and B. L. Liu, "Optimization of the low coherence and high robustness observation matrix," *Journal of Xidian University*, vol. 46, no. 6, pp. 171–178, 2019.

[12] G. Reeves and H. D. Pfister, "The replica-symmetric prediction for compressed sensing with Gaussian matrices is exact," in *Proceedings of the 2016 IEEE International Symposium on Information Theory (ISIT)*, pp. 665–669, Barcelona, Spain, July 2016.

[13] T. Huang, Y. Z. Fan, and M. Hu, "Compressed sensing based on random symmetric Bernoulli matrix," in *Proceedings of the 2017 Youth Academic Conference of Chinese Association of Automation (YAC)*, pp. 191–196, Hefei, China, May 2017.

[14] E. P. K. Gillert, B. Kaliaperumal, E. B. Rajsingh, and M. Lydia, "Trust based data prediction, aggregation and reconstruction using compressed sensing for clustered wireless sensor networks," *Computers and Electrical Engineering*, vol. 72, pp. 894–909, 2018.

[15] Y. Luo, J. J. Dang, Z. X. Song, and B. P. Wang, "Construction and Performance research of discrete chaotic measurement matrix," *Systems Engineering and Electronics*, vol. 42, no. 4, pp. 749–755, 2020.

[16] S. Rapuano, "Analog-to-Information converters: research trends and open problems," in *Proceedings of the 2016 26th International Conference Radioelektronika (RADIOELEKTRONIKA)*, pp. 1674–1677, Kosice, Slovakia, April 2016.

[17] J. Laska, S. Kirolos, Y. Massoud et al., "Random sampling for analog-to-information conversion of wideband signals," in *Proceedings of IEEE International Conference on Design, Applications, Integration and Software (DCAS)*, pp. 119–122, Richardson, TX, USA, October 2006.

[18] D. Adams, Y. C. Eldar, and B. Murmann, "A mixer front end for a four-channel modulated wideband converter with 62-dB blocker rejection," *IEEE Journal of Solid-State Circuits*, vol. 52, no. 5, pp. 1286–1294, 2017.

[19] Y. Zhao, H. Wang, X. Zhuang, Z. Dai, and H. Wu, "Frequency domain sensing system using random modulation pre-integrator," *IET Science, Measurement and Technology*, vol. 7, no. 3, pp. 166–170, 2013.

[20] H. Mamaghanian, N. Khaled, D. Atienza, and P. Vandergheynst, "Design and exploration of low-power analog to information conversion based on compressed sensing," *IEEE Journal on Emerging and Selected Topics in Circuits and Systems*, vol. 2, no. 3, pp. 493–501, 2012.

[21] R. Wang, J. Guo, and H. Leung, "Orthogonal circulant structure and chaotic phase modulation based analog to information conversion," *Signal Processing*, vol. 144, no. 3, pp. 104–117, 2018.

[22] W. Xu, Y. Cui, Y. Wang, S. Wang, and J. Lin, "A hardware implementation of random demodulation analog-to-information converter," *IEICE Electronics Express*, vol. 13, no. 16, pp. 1–6, 2016.

[23] H. Rauhut, J. Romberg, and J. A. Tropp, "Restricted isometries for partial random circulant matrices," *Applied and Computational Harmonic Analysis*, vol. 32, no. 2, pp. 242–254, 2012.

[24] E. Candès and J. Romberg, "Sparsity and incoherence in compressive sampling," *Inverse Problems*, vol. 23, no. 3, pp. 969–985, 2007.

[25] J. H. Wang, H. Z. Tao, Y. Y. Zhou, and F. H. Wang, "Generalized incoherence principle in compressed sensing," *Signal Processing*, vol. 28, no. 5, pp. 675–679, 2012.

[26] A. S. Ali, A. G. Radwan, and A. M. Soliman, "Fractional order butterworth filter: active and passive realizations," *IEEE Journal on Emerging and Selected Topics in Circuits and Systems*, vol. 3, no. 3, pp. 346–354, 2013.

[27] M. C. Tripathy, D. Mondal, K. Biswas, and S. Sen, "Experimental studies on realization of fractional inductors and fractional-order bandpass filters," *International Journal of Circuit Theory and Applications*, vol. 43, no. 9, pp. 1183–1196, 2015.

[28] L. A. Said, S. M. Ismail, A. G. Radwan, A. H. Madian, M. F. Abu El-Yazeed, and A. M. Soliman, "On the optimization of fractional order low-pass filters," *Circuits, Systems, and Signal Processing*, vol. 35, no. 6, pp. 2017–2039, 2016.

[29] Y. Han, Y. Feng, P. Yang, L. Xu, Y. Xu, and F. Blaabjerg, "Cause, classification of voltage sag, and voltage sag emulators and applications: a comprehensive overview," *IEEE Access*, vol. 8, pp. 1922–1934, 2019.

[30] A. Kalair, N. Abas, A. R. Kalair, Z. Saleem, and N. Khan, "Review of harmonic analysis, modeling and mitigation techniques," *Renewable and Sustainable Energy Reviews*, vol. 78, pp. 1152–1187, 2017.